Resonance Raman Study of Ferric Heme Adducts of Dehaloperoxidase from *Amphitrite ornata*†

Jennifer Belyea, Curtis M. Belyea, Simon Lappi, and Stefan Franzen*

Department of Chemistry, North Carolina State University, Raleigh, North Carolina 27695

Received May 10, 2006; Revised Manuscript Received September 26, 2006

ABSTRACT: The study of axial ligation by anionic ligands to ferric heme iron by resonance Raman spectroscopy provides a basis for comparison of the intrinsic electron donor ability of the proximal histidine in horse heart myoglobin (HHMb), dehaloperoxidase (DHP), and horseradish peroxidase (HRP). DHP is a dimeric hemoglobin (Hb) originally isolated from the terebellid polychaete *Amphitrite ornata*. The monomers are structurally related to Mb and yet DHP has a peroxidase function. The core size marker modes, ν_2 and ν_3, were observed using Soret excitation, and DHP-X was compared to HHMb-X for the ligand series X = F, Cl, Br, SCN, OH, N_3, and CN. Special attention was paid to the hydroxide adduct, which is also formed during the catalytic cycle of peroxidases. The Fe−OH stretching frequency was observed and confirmed by deuteration and is higher in DHP than in HHMb. The population of high-spin states of the heme iron in DHP was determined to be intermediate between HHMb and HRP. The data provide the first direct measurement of the effect of axial ligation on the heme iron in DHP. The Raman data support a modified charge relay in DHP, in which a strongly hydrogen-bonded backbone carbonyl (>C═O) polarizes the proximal histidine. The charge relay mechanism by backbone carbonyl >C═O-His-Fe is the analogue of the Asp-His-Fe of peroxidases and Glu-His-Fe of flavohemoglobins.

Dehaloperoxidase (DHP)[1] is an enzyme native to the terebellid polychaete *Amphitrite ornata* that has peroxidase activity and a globin fold (*1*, *2*). DHP is a dimeric Hb consisting of eight α-helices (a−h) and a protoporphyrin IX prosthetic group (*3*, *4*) with a central metal atom that reversibly binds diatomic ligands such as molecular oxygen (O_2), carbon monoxide (CO), and nitric oxide (NO) (*5*−*8*). DHP bears a resemblance to dimeric Hbs such as *Ascaris scarpharca* Hb (*9*) and cytoglobin (*10*). However, the dual function of DHP appears to be unique in the known evolution of globins (*4*, *11*, *12*). The peroxidase activities of typical globins have been characterized and are known to have turnover numbers that are more than 100 times smaller than those of horseradish peroxidase (HRP) (*13*−*16*). Recently, DHP has been expressed and purified in a recombinant form in *Escherichia coli* (*5*), and the enzymatic rate for conversion of trihalogenated phenols to dihalogenated quinone by DHP is 12 times slower than that of HRP and 13 times faster than that of horse heart myoglobin (HHMb). In spite of the low structural homology with peroxidases, DHP clearly has a peroxidase function. However, the fact that DHP apparently binds the substrate in an internal binding site suggests that a two-electron oxidation mechanism is an important pathway for oxidation of the substrate (*3*, *4*).

Comparison of the proximal histidine structures of HHMb, DHP, and HRP poses a question regarding the catalytic mechanism of DHP. DHP resembles a Hb much more than it does a peroxidase in the hydrogen bonding of the proximal histidine. Specifically, peroxidases are known to have strong hydrogen bonding to a negatively charged aspartate (*17*−*22*). The recently discovered class of bacterial flavohemoglobins also has a strong hydrogen bond of the proximal histidine to glutamate (*23*). This strong hydrogen bonding leads to a greater negative charge on the imidazole ring ligated to the heme iron. The charge relay comprised by the Asp-His-Fe catalytic triad permits higher oxidation states of iron to be formed, consistent with the requirement for the formation of compound I. DHP lacks this feature (*24*), although the proximal histidine of DHP does form a strong hydrogen bond with the carbonyl group of Leu83 (*25*, *26*). This hydrogen bonding does not, at first, appear significantly different from the bifurcated hydrogen bond in myoglobin that involves a weak interaction with the lone pair of Ser92 and an interaction with carbonyl group of Ile89. Attempts to engineer myoglobin by means of the Ser92Asp mutation that would introduce a charge relay do not produce a significant increase in peroxidase activity (*27*, *28*). DHP may have evolved a different more subtle charge relay that permits it to function both as a globin and as a peroxidase. In DHP, the Leu93-C═O···Nδ-His89 hydrogen bond length is 2.9 Å, which is significantly shorter than the corresponding hydrogen bond in myoglobin (*3*, *4*). It is still not understood how the >C═O-His-Fe catalytic triad facilitates peroxide activation in DHP that is analogous to the Asp-His-Fe charge relay in peroxidases.

† S.F. acknowledges support through NSF Grant MCB-9874895.

* Corresponding author. E-mail: Stefan_Franzen@ncsu.edu. Phone: (919) 515-8915. Fax: (919) 515-8920.

[1] Abbreviations: DHP, dehaloperoxidase; Hb, hemoglobin; HHMb, horse heart myoglobin; HRP, horseradish peroxidase; HS, high spin; IS, intermediate spin; LS, low spin; SWMb, sperm whale myoglobin; SVD, singular value decomposition.

10.1021/bi0609218 CCC: $33.50
Published on Web 11/07/2006

Scheme 1: Depiction of the Geometry of Distal and Proximal Side Hydrogen Bonding for Hydrogen Bond Acceptor Ligand X and for Hydroxide[a]

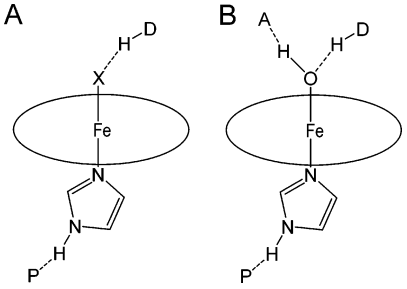

[a] The P moiety on the proximal side is a hydrogen bond acceptor [e.g., −COO−, −O (lone pair), =C=O]. The D−H moiety on the distal side is a hydrogen bond donor (e.g., N−H from histidine or arginine). The A moiety on the distal side is a hydrogen bond acceptor such as the histidine lone pair or the lone pair from an oxygen on water.

The ligation strength of the proximal histidine should be directly correlated with the charge supported on the heme iron and inversely correlated with the spin state of the iron. The spin states of ferric heme proteins are $S = {}^1/_2$, $S = {}^3/_2$, and $S = {}^5/_2$, which will be referred to as LS, IS, and HS, respectively. The greater the basicity of the axial ligand, the higher the energy of the d_{z^2} and d_π (d_{xz}, d_{yz}) orbitals, due to σ- and π-bonding interactions, respectively. The charge density in the ligand field causes these d-orbitals to increase in energy and consequently lowers the spin state (*29*). In addition to effects of axial ligation on spin state, the axial ligands (F^-, Cl^-, Br^-, OH^-, SCN^-, N_3^-, and CN^-) can have differential effects on the Soret band spectrum depending on the mixing of the π-system of the ligand. While one can compare the native ferric state, this is complicated by the fact that water is ligated in ferric HHMb but not ferric HRP (*18*, *19*, *30*). The situation is still under investigation for DHP since the X-ray crystal structure shows the heme to be 5-coordinate (*3*, *4*), but magnetic circular dichroism (*31*) and UV−vis titrations (*6*) suggest that water may be bound in the ferric form. This type of comparison is complicated in part by distal interactions and hydrogen-bonding interactions (*32*−*35*).

On the distal side peroxidases and globins both have a prominent histidine, known as the distal histidine. However, peroxidases also have a highly conserved arginine that is thought to stabilize proton transfer essential to rapid activation of bound peroxide to form compound I (*13*, *18*, *19*, *30*, *36*−*38*). However, bound hydroxide presents an especially interesting situation since there are both hydrogen bond donor and acceptor interactions. Depending upon the nature of the hydrogen-bonding groups in the distal pocket, the Fe−OH bond can either be strengthened or weakened by interactions in the distal pocket. A hydrogen bond donor interaction with a σ-bonding distal ligand acts as a charge relay in reverse and reduces the ligation strength of the bound ligand. The situation for π-bonding ligands such as CO is more complex due to the competition between σ-donation and π-back-bonding (*39*). The proximal and distal charge relays are illustrated in Scheme 1.

The distal and proximal differences between globins and peroxidases can be related to their functional differences. In peroxidases, the greater negative charge on the proximal histidine Nϵ that arises due to the interaction of Nδ with a hydrogen-bonding aspartate (*17*, *24*) results in a greater tendency for low-spin iron, which reduces the core size of the iron. The greater ligation strength leads to a "push" at the heme iron that is thought to be necessary for peroxidase activation (*40*). Specifically, compound I formation is facilitated by the strong proximal histidine ligation, which stabilizes LS iron and the Fe(IV) oxidation state of the iron required for compounds I and II. Globins have a weaker ligation between the proximal histidine and the iron, resulting in a greater population of the HS state (*41*). A structural displacement of the heme iron out of the heme plane in the high-spin state gives rise to the domed conformation in globins. DHP is predicted to have spin states and iron charge values that are between globins and peroxidases based on axial ligation discussed above and based on the observed reactivity, which is intermediate between HRP and HHMb. Commensurate with this expectation, the ν_{Fe-His} frequency in ferrous deoxy-DHP is observed at 233 cm^{-1} (*8*), which is intermediate between HHMb $\nu_{Fe-His} = 221$ cm^{-1} (*42*) and HRP $\nu_{Fe-His} = 243$ cm^{-1} (*17*). One of the goals of the present study is to test whether the trends in the spin states of ferric heme of the three proteins, HHMb, DHP, and HRP, are analogous to the ligation strength for ferrous heme.

The distal pocket structure of DHP has important differences with respect to both globins and peroxidases. The Nϵ−H of distal histidine in peroxidase is 1.5 Å farther away from the iron heme than in that of globins (*18*, *20*−*22*), which affects both function and spectroscopy (*33*). In peroxidases, the greater distance allows the histidine to provide a "pull" to activate the cosubstrate, hydrogen peroxide (*43*). Formation of compound I in peroxidases is accomplished by the distal histidine with the aid of an arginine residue that is absent in DHP (*13*, *36*−*38*). In globins, the distal histidine hydrogen bonds with the diatomic ligand to stabilize the bound ligand but does not have any auxiliary hydrogen-bonding partners (*39*, *44*, *45*). The distal histidine in DHP, His55, is positioned 1.5 Å further from the heme iron and therefore has spatial similarity with the peroxidase geometry (*3*, *4*) but is apparently not capable of strong hydrogen bonding to bound CO (*6*, *8*). His55 has two conformations in the DHP X-ray crystal structures (*3*, *4*). The terms "open" and "closed" conformations correspond to a solvent-exposed and internal conformation, respectively, for the distal histidine in Mb (*46*). The open or solvent-exposed conformation of H64 is observed at pH ~4.5 in Mb (*47*). While there is an analogy with DHP, the open conformation in DHP is observed at much higher pH. According to the crystallization conditions the open form is in equilibrium with the closed form at pH 6.5 (*3*, *4*). Moreover, when substrate is present, the histidine is in the open conformation (*3*, *4*). The functional consequence of the two conformations of the distal histidine is not known, but it is clear that His55 in DHP would need to be in the closed conformation to participate in hydrogen bonding with a ligand bound to the heme iron as well as for catalysis of Fe−H_2O_2 to form compound I since it is located more than 9 Å from the heme iron in the open conformation. Mutants in the His55 position result in severely reduced enzymatic acdtivity in DHP (*48*). The ferric liganded heme species studied here are probes of the distal pocket polarity as shown in Scheme 1. The interactions of the amino acid residues in the distal pocket with bound ligands can affect the core size

marker modes by modulating the ligation strength. The effect of hydrogen bonding by residues in the distal pocket is particularly noticeable for the weak ligand field of fluoride (*49*).

Resonance Raman spectroscopy provides information on the axial ligand vibrations and the effect of axial ligation on heme structure. The interplay of axial ligation and heme geometry can be monitored by observation of three Raman bands known as the core size marker bands, ν_3, ν_2, and ν_{10}, in the 1470−1510, 1560−1580, and 1610−1640 cm^{-1} regions, respectively, of the resonance Raman spectrum. These vibrations arise from motions on the heme periphery, but their frequencies are sensitive to strain induced by the iron that depends upon the distribution of d-electrons (*50*, *51*). Since the axial ligand field has a strong effect on the iron spin state, the core size modes report on the strength of axial ligation. The ν_2 and ν_3 modes are of A_{1g} symmetry in a simplified D_{4h} model of the heme. These modes are Frank−Condon active and most intense for Soret band excitation. The ν_{10} mode has B_{1g} symmetry and is most intense for Q-band excitation. In ferric heme each core size marker appears as a pair of bands that correspond to two populations of spin states in equilibrium. We have found that the core size marker band ν_3 is the most reliable indicator of the relative population of each spin state because it is an isolated region of the Raman spectrum. At wavenumbers greater than 1600 cm^{-1} where ν_{10} is observed, the spectrum is complicated by the presence the heme vinyl modes $\nu_{C=C}$ (*49*, *52*). The ν_2 band is also in a spectrally congested region together with bands ν_{11}, ν_{19}, and ν_{35} (*52*).

Although both globins and peroxidases have the same protoporphyrin IX prosthetic group, the heme geometries differ due to restrictions enforced by protein structure (*53*). Globins have been shown to have both a planar and domed heme conformation (*25*). Ferrous 6-coordinate hemes have a planar conformation consistent with an iron spin of $S = 0$. A domed conformation has a 5-coordinate heme iron consistent with a spin of $S = 2$. The transition from low to high spin of the ferrous heme in globins can be monitored by Raman spectroscopy (*54*−*56*). Saddling of the heme is observed in peroxidases. The changes in heme structure for various ligation states are less pronounced in peroxidases than in globins. In 6-coordinate adducts both LS and HS forms are possible depending on the strength of the axial ligand field. The 5-coordinate heme in peroxidase may be a mixed- or intermediate-spin state, IS, or HS. The spin state is an important observable for understanding the strength of axial ligation and the role it plays in supporting the Fe(IV) oxidation state of iron required for formation of compounds I and II. Moreover, the spin state is a crucial for understanding enzymatic activity observable because it is the consequence of the charge relay discussed above. The presence of a mixed-spin state in peroxidases is likely a functional consequence of the strong axial ligation since 5-coordinate adducts would normally be expected to be high spin. Since DHP is a globin peroxidase, the present study focuses on the role of ferric spin states in a domed heme that structurally resembles myoglobin rather than a typical peroxidase. We will address the spectroscopic similarities as a probe of the active site bonding and electronic structure.

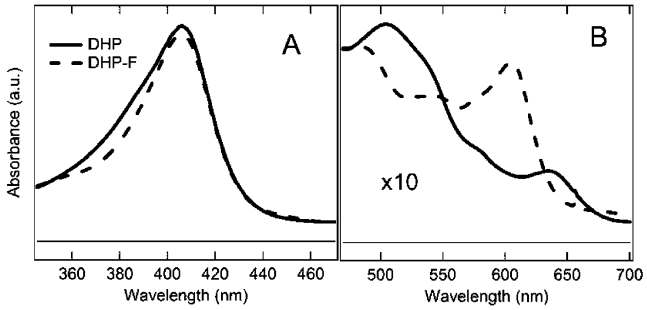

FIGURE 1: Absorption Soret spectra of high-spin ferric DHP (solid line) and ferric DHP with fluoride ligand (dash line) in 100 mM phosphate buffer, pH 6.0 at room temperature. (A) Soret maxima for both the ferric DHP and ferric DHP-F are 406 nm with small differences in the bandwidths. (B) The Q-bands and charge-transfer bands (*64*) of ferric DHP and ferric DHP-F are shown.

MATERIALS AND METHODS

Absorption Spectroscopy. DHP samples were purified from *E. coli* according to published methods (*5*). Protein was dialyzed against water to remove all salts and concentrated using Millipore Ultra-4 centrifugal filters, WMCO 10000. Concentrated samples were flash frozen using liquid nitrogen or dry ice and then lyophilized using a Labconco Freezer Dryer 4.5. DHP samples were prepared by dissolving lyophilized DHP in water at a final concentration of 6 μM. Excess potassium ferricyanide was added to the protein solution to oxidize the iron heme to the ferric state. Excess oxidant was removed by size exclusion chromatograpy using a Sephadex G-25 column (Sigma-Aldrich G2580-10G). Protein was collected and concentrated in Millipore Amicon Ultra-4 MWCO 10000. A buffer exchange was performed in the Amicon Ultra-4 so the resulting protein solutions were buffered in 100 mM citrate, pH 6.0, and 100 mM carbonate, pH 10.5. Lyophilized horseradish peroxidase was purchased from Fluka (EC 1.11.1.7), and lyophilized horse heart myoglobin was purchased from Sigma (CAS M1882). Both horseradish peroxidase and horse heart myoglobin were used without further purification. Lyophilized HHMb and HRP proteins were dissolved in 100 mM citrate buffer, pH 6.0, or 100 mM borate buffer, pH 10.5.

Absorption spectra were recorded using a Hewlett-Packard 8453 multiwavelength spectrometer. The ferric DHP in 100 mM citrate buffer, pH 6.0, had a Soret band maximum at 406 nm and a broad Q-band from 550 to 575 nm, as shown in Figure 1. In order to produce ligated protein samples, aliquots of concentrated ligand solutions were added, and the Soret and Q-band shifts were measured. Addition of ligand was done quantitatively up to concentrations of 500 mM to ensure that spectroscopic changes associated with the binding of each ligand were observed. It was determined that 50 mM of each of the ligands F^-, Cl^- Br^-, SCN^-, N_3^-, and CN^- was sufficient to produce a 6-coordinate adduct, and this concentration was used for the data reported in Table 1.

Protein Samples for Resonance Raman Experiments. Lyophilized proteins were dissolved in 0.5 M ligand and 100 mM citrate, pH 6.0, with the final concentration of protein of 120 μM. Ligands used were obtained from the dissolved salts of KF, NaCl, KBr, KSCN, KCN, and NaN_3 at concentrations of 50 mM. Carbonate buffer (100 mM) with a pH of 10.5 was used to obtain the hydroxide ligand. Each

Table 1: Soret Maxima for Ferric HHMb, DHP, and HRP Ligated Samples[a]

	λ max (nm)		
ligand	Mb Soret	DHP Soret	HRP Soret
none	407	406	403
F^-	407	406	404
Cl^-	409	406	
Br^-	409	406	
SCN^-	412	413	
OH^-	413	414	415
N_3^-	420	421	413
CN^-	423	423	422

[a] All samples were made in 100 mM citrate buffer, pH 6, with 50 mM concentration of the respective anionic ligand.

protein/ligand combination (200 μL) was placed into a separate 5 mm diameter glass NMR tube. Samples were stored on ice until used.

Resonance Raman Spectroscopy. Resonance Raman spectra were obtained by excitation at the edge of the Soret band at 410 or 424 nm using Coherent Verdi laser (N10-A1654), generating 10 W of 532 nm light which was used to power a Coherent Mira 900 to generate 820 and 840 nm light. The resulting beam was sent through a Coherent 5-050 doubler (01088) to generate 410−430 nm light as the excitation source for the resonance Raman experiments. The laser output was calibrated using Rayleigh scattering, toluene and cyclohexane standards, and lines from Kr and Ar lamps. The excitation source was collimated and cylindrically focused to a vertical line of ∼0.5 mm and typically 45−60 mW at the sample. Raman scattered light passed through a Spex 1877 Triplemate monochromator and was detected by a liquid N_2-cooled CCD camera (ISA Spex, model CCD-3000). Samples were placed in 5 mm NMR tubes and spun with an air piston spinning sample holder (Princeton Photonics, model Raman 101). Spectra were measured at room temperature for three acquisitions with exposure times of 180 s, alternating between samples to minimize sample degradation. Each sample scan was repeated four to eight times to improve the signal-to-noise ratio.

Fits of the resonance Raman spectra to a Gaussian fitting model were performed using Igor Pro 5.0. The results of the fits are represented in Tables 2−5. Each Gaussian is

$$G(\omega) = \frac{A}{\sqrt{2\pi}\sigma} \exp\left[-\frac{(\omega - \omega_0)^2}{2\sigma}\right] \quad (1)$$

The parameters in Tables 2−5 correspond to A, ω, and σ for both of the modes ν_2 and ν_3. The percentage of high spin, HS, was determined for ν_3 and ν_{10} using the equation:

$$\%\ \mathrm{HS} = \frac{(A/\sigma)_{\mathrm{HS}}}{(A/\sigma)_{\mathrm{LS}} + (A/\sigma)_{\mathrm{HS}}} \quad (2)$$

Density Functional Theory Calculations. The model system used in this study consisted of a 5-coordinate iron−porphine−imidazole. The optimized ground state geometries at three spin states were obtained using the GGA functional (*57*) as implemented in DMol3 (Accelrys Inc.) (*58*, *59*). All calculations were carried out on a PQS QuantumCube computer. Geometry optimizations were carried out without constraints until the energy difference was less than 10^{-6} au on subsequent iterations. Numerically tabulated basis sets of double-ζ plus extra polarization (DNPP) quality were employed as described in the Supporting Information. For the DNPP basis there are four basis functions for H (1s, 2s, 2p, 3d) and seven basis functions for C, N, and O [1s, 2s(2), 2p(2), 3d, 4f]. The potential energy surfaces were calculated using the Thermal option (grand canonical ensemble) treatments of the density functional (*60*) as reported elsewhere (*39*, *61*−*63*). The grand canonical (Thermal) option always converged to a lower overall energy. The grand canonical calculation was carried out at an electronic temperature of $k_BT = 0.02$ eV. Once a calculation was complete, it was extrapolated to zero temperature by subtraction of the thermal electron occupation according to the grand canonical partition function.

Table 2: Results of Gaussian Fits to Resonance Raman Data Collected for Ferric 6-Coordinate DHP Adducts[a]

	ν_3 HS	ν_3 LS	ν_2 HS	ν_2 LS
DHP-F				
ω	1475	1503	1560	1584
σ	9.68	8.84	16.6	10
%	65	35	41	59
DHP-Cl				
ω	1487	1503	1561	1584
σ	9.6	8	20.9	13.8
%	36	64	35	65
DHP-Br				
ω		1504	1557	1583
σ		7.8	10.1	13.3
%		100	27	73
DHP-SCN				
ω	1471	1502	1552	1582
σ	9.9	8.4	15.3	15.1
%	9	91	21	79
DHP-N_3				
ω	1476	1503	1560	1584
σ	11.3	8	15.5	14.2
%	21	79	40	60
DHP-OH				
ω	1476	1502	1552	1582
σ	10.2	8.4	15.7	17.3
%	32	68	31	69
DHP-CN				
ω		1502	1556	1582
σ		8.8	18.5	13.4
%		100	19	81

[a] The parameters are ω (position) and σ (Gaussian width), and % is percentage HS or LS as calculated using eqs 1 and 2.

RESULTS

The absorption and resonance Raman spectra are presented for the ferric adducts of DHP. Experiments were performed on both HHMb and HRP for comparison. The ferric hydroxyl adduct was studied in particular detail to establish the nature of acid−alkaline transition.

Absorption Spectroscopy. Absorption spectra were obtained for the entire series of ferric adducts ranging from no ligand (DHP) to the strongest ligand, cyanide (DHP-CN). Figure 1 shows the absorption spectra for ferric DHP with and without bound fluoride ligand. The Soret band and Q-band are shown in panels A and B of Figure 1, respectively. The Q-band region shown in panel B reveals the presence of a charge-transfer band at 605 nm upon the addition of fluoride ligand to ferric DHP to make DHP-F (*64*). The Soret maxima for both ferric DHP and DHP-F are

Table 3: Results of Gaussian Fits to Resonance Raman Data Collected for Ferric 6-Coordinate HHMb Adducts[a]

	ν_3 HS	ν_3 LS	ν_2 HS	ν_2 LS
HHMb-H_2O				
ω	7	6.6	16.5	16.5
σ	1481	1516	1560	1580
%	67	33	50	50
HHMb-F				
ω	1476	1508	1557	1580
σ	6.8	5.2	12.6	8.9
%	71	29	72	28
HHMb-Cl				
ω	1476	1508	1558	1580
σ	6.6	4.9	12.6	8.5
%	70	30	72	28
HHMb-Br				
ω	1480	1512	1563	1583
σ	7.2	3.65	10.9	6.5
%	74	26	81	19
HHMb-SCN				
ω	1473	1507	1558	1580
σ	6	5.1	14.2	10.2
%	72	28	65	35
HHMb-N_3				
ω	1469	1499	1552	1579
σ	7.3	7.4	15.5	11.3
%	23	77	26	74
HHMb-OH				
ω	1486	1502	1553	1580
σ	8.6	3.8	13.7	12
%	83	17	33	67
HHMb-CN				
ω		1506		1585
σ		6.2		14
%		100		100

[a] The parameters are ω (position) and σ (Gaussian width), and % is percentage HS or LS as calculated using eqs 1 and 2.

Table 4: Results of Gaussian Fits to Resonance Raman Data Collected for Ferric 6-Coordinate HRP Adducts[a]

	ν_3 HS	ν_3 LS	ν_2 HS	ν2 LS
HRP-F				
ω	1479	1505	1567	1582
σ	8.8	10.2	15.3	5.9
%	94	6	44	56
HRP-OH				
ω	1479	1504	1562	1585
σ	11.3	6.7	6.9	10.3
%	23	77	36	64
HRP-CN				
ω	1477	150		1585
σ	21.4	7.3		16.8
%	5	95		100

[a] The parameters are ω (position) and σ (Gaussian width), and % is percentage HS or LS as calculated using eqs 1 and 2.

both at 406 nm, which is characteristic of the mostly high-spin (HS) form of the heme iron expected for both met and fluoride adducts. The addition of fluoride ligand has little effect on the Soret band maximum and intensity but does result in a slight narrowing of the Soret band.

The absorption spectra of OH^-, N_3^-, and CN^-adducts of ferric DHP are presented in Figure 2. As ligand strength in ferric adducts of DHP increases, there are shifts in the Soret band maxima from 406 to 423 nm. Table 1 provides a summary of the Soret maxima for DHP, HRP, and HHMb. It was difficult to detect binding of the Cl^-, Br^-, and SCN^- ligands to HRP by either UV−vis or Raman spectroscopy, and therefore these values are not reported. Figure 2A illustrates the shift in the Soret maxima that arises from the increasing ligation strength of the ligand, which includes both effects on spin state and the π-acid character (*65*, *66*). Figure 2B shows the changes in the Q-band spectral region that are consistent with the change from high to low spin. The spectra of the three adducts shown in Figure 2B all have α and β bands at 550 and 575 nm, respectively. DHP-OH and DHP-N_3 adducts have additional charge-transfer bands at 603 and 640 nm, respectively.

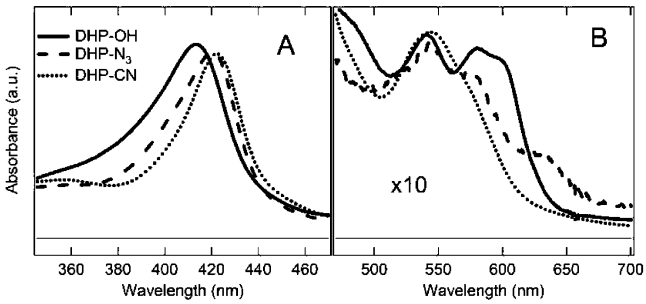

FIGURE 2: Absorption spectra of mixed and low-spin ferric DHP samples. (A) The shift in the Soret band maximum from 406 nm for ferric DHP to 414, 421, and 423 nm for hydroxide (solid line), azide (dash line), and cyanide (dotted line) ferric DHP, respectively, is characteristic of mixed to low-spin forms of ferric DHP. (B) The Q-(α/β)-band and charge-transfer band spectra (*64*) are shown.

Table 5: Results of Gaussian Fits to Resonance Raman Data Collected for Ferric 5-Coordinate Adducts[a]

	ν_3 IS	ν_2 IS
HRP		
ω	1498	1577
σ	16	19.3
DHP		
ω	1502	1582
σ	6.5	12.5

[a] The parameters ω (position) and σ (Gaussian width) were calculated using eqs 1 and 2.

The pK_a for formation of the hydroxide adduct of DHP was determined from the pH dependence of the Soret band. A pK_a of 8.0 was determined for ferric DHP, which is in agreement with earlier pK_a determination of 8.1 (*6*). The data are provided in the Supporting Information for comparison with Mb and HRP. In globins where water is bound to the heme iron at low pH this transition is known as the acid−alkaline transition. However, the crystal structure for DHP reveals no water bound in the ferric form of the enzyme. These data and the data presented elsewhere suggest that the low-pH form may be metaquo DHP rather than 5-coordinate ferric DHP. The high pH form is clearly ferric hydroxyl DHP (DHP-OH).

Resonance Raman Spectra. Resonance Raman spectra were obtained for aqueous ferric DHP and ferric DHP bound to anionic ligands. The core size marker modes ν_2 and ν_3 were used for the analysis of HS and LS population since these modes are intense enough for all of the ligated proteins to be measured. The ν_3 is located in the range from 1470 to 1510 cm^{-1} for DHP and is the most isolated core size marker mode. On the basis of the data obtained here, ν_3 appears to be the most reliable Raman band for the determination of the two spin state populations, LS and HS.

The resonance Raman spectra of ferric DHP, HRP, and HHMb are shown in Figure 3 with the Gaussian fits to the

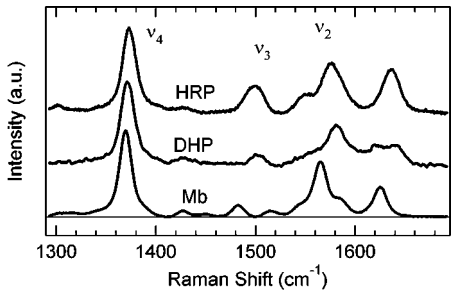

FIGURE 3: RR spectra are shown in the high-frequency region for the ferric forms of HHMb, DHP, and HRP at pH 6.0. The Raman excitation wavelength was 410 nm.

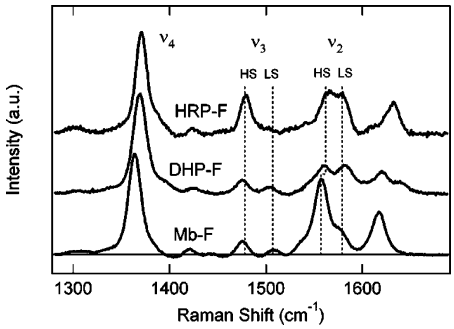

FIGURE 4: RR spectra are shown in the high-frequency region for the fluoride adducts of HHMb, DHP, and HRP. The Raman excitation wavelength was 410 nm.

ν_2 and ν_3 modes given in Table 5. Ferric HHMb has water bound to the iron, which is also known as metaquo, and is thus 6-coordinate. The metaquo form of HHMb has two ν_3 Raman bands at 1481 and 1514 cm^{-1} whose intensities are proportional to the relative population of 67% HS and 33% LS, respectively. The 5-coordinate ferric HRP does not have the same frequency as 6-coordinate forms, and this has been ascribed to an IS or IS, HS-mixed state (*67*). Figure 3 shows that the ν_3 in DHP is observed at 1502 cm^{-1} and has strong resemblance to the HRP ν_3 mode. This observation could arise from a mixed spin iron due to a 5-coordinate heme as suggested by the X-ray structure to the iron or from a heme-bound water that has significant hydrogen-bonding contributions shown in Scheme 1.

The fluoride adduct has the greatest population of the high-spin state of all the ligands for all three proteins. In Figure 4, the ν_3 high-spin peaks are observed at 1475, 1476, and 1479 cm^{-1} for DHP-F, HHMb-F, and HRP-F. Low-spin ν_3 peaks are observed at 1503, 1508, and 1504 cm^{-1} for DHP-F, HHMb-F, and HRP-F, respectively. HRP-F has more high-spin character than HHMb-F and DHP-F. HRP-F has 94% HS as calculated from ν_3 where DHP-F HS is 65% and HHMb-F HS is 70%.

Cyanide is the typical ligand used to induce the LS iron for heme proteins. Tables 2−4 present the Raman data obtained for DHP-CN, HHMb-CN, and HRP-CN. The low-spin ν_3 is at 1504, 1506, and 1506 cm^{-1} for DHP-CN, HHMb-CN, and HRP-CN, respectively. DHP-CN and HHMb-CN are 100% LS and HRP-CN is 95% LS as calculated from ν_3.

The fluoride and cyanide adducts represent the two extremes of 6-coordinate HS and LS, respectively. In HHMb there is a transition as measured by ν_3 from mainly HS (Cl^-, Br^-, SCN^-, OH^-) to mostly LS (N_3^- and CN^-) as ligand

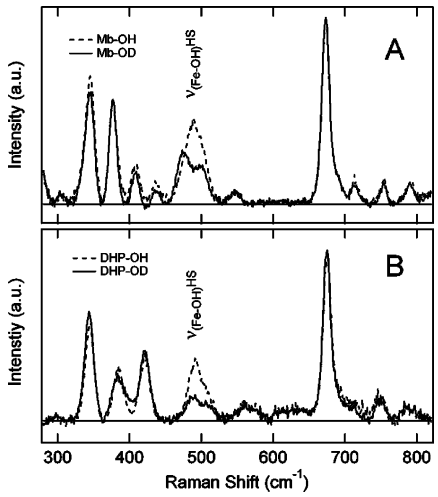

FIGURE 5: RR spectra collected for the lower window of the hydroxide adducts. Sample conditions are 120 μM protein dissolved in 0.025 M borate buffer, pH 10.5 or pD 10.9. The Raman excitation wavelength was 410 nm. (A) The Raman data for the Mb-OH sample are shown. (B) The Raman data for the DHP-OH sample are shown. For both samples the spectra are shown as OH (dashed line) and OD (solid line).

strength increases. In DHP the transition to LS occurs already for the much more weakly ligating halogens. Chloride-ligated DHP is 64% LS, compared to 30% LS for HHMb-Cl. DHP-Br is 100% LS, while HHMb-Br was only 26% LS based on the analysis of ν_3. The resonance Raman data for these ligands are presented in the Supporting Information. The core size of DHP does appear to show a trend for the halogens in which the percentage of HS is 65%, 36%, and 0% for F^-, Cl^-, and Br^-, respectively. There is precedent for the chloride and bromide adducts in protohemin (*68*). The trends in the Soret band for the halide adducts of DHP shown in Table 1 do not follow the trend of spin states in Table 2 but rather are relatively constant. The DHP-SCN adduct is primarily LS, while the HHMb-SCN adduct has significant HS character, yet both show similar Soret band maxima of 412−413 nm. The azide adducts DHP-N_3 and HHMb-N_3 have similar percentages of HS character, 21% and 23%, and have Soret bands that are in the range 420−421 nm. These observations suggest that factors other than spin state are governing the position of the Soret band maximum in both HHMb and DHP.

The hydroxide adduct of DHP is representative of a mixed-spin heme protein; DHP-OH is 68% LS and 32% HS as measured by ν_3 data in Table 2. The hydroxide derivative of ferric Mb was previously determined to exist in thermal spin-state equilibrium at room temperature with 30% LS and 70% HS (*69*, *70*). On the basis of ν_3, the HHMb-OH data in Table 2 indicate a 17% LS and 83% HS mixture. HRP-OH has been shown to exist in a 93% LS and 7% HS equilibrium at room temperature (*70*−*72*). On the basis of these data DHP-OH has a spin population that lies almost exactly halfway between those of HHMb-OH and HRP-OH.

The axial vibrations of the ferric−hydroxyl adduct is readily observable and can be verified using deuteration as shown in Figure 5. In Figure 5A a ν_{Fe-OH} stretching mode has been identified for HHMb-OH at 489 cm^{-1} with a smaller Raman mode at 506 cm^{-1} of unknown origin. The isotope effect and temperature dependence of SWMb-OH have been studied previously and are nearly identical to the data

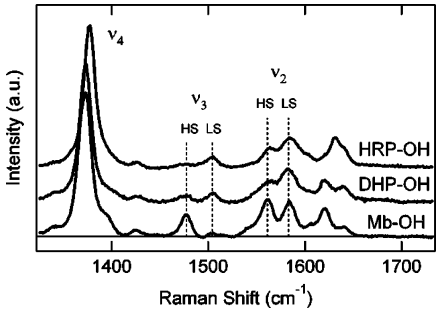

FIGURE 6: RR spectra are shown in the high-frequency region for the hydroxy adducts HHMb-OH, DHP-OH, and HRP-OH. The HRP-OH and Mb-OH samples were prepared at pH 12.0. The DHP-OH sample was prepared at pH 10.5. The Raman excitation wavelength was 410 nm.

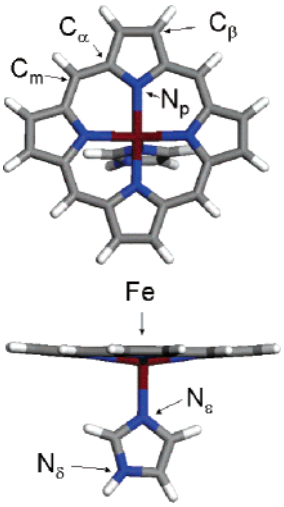

FIGURE 7: A representation of ferric iron porphine used for model DFT calculations. The identities of key atoms in the structure are given for reference with the text.

obtained here (*70*). The corresponding DHP-OH mode is observed at 491 cm^{-1} with a mode of unknown origin at 513 cm^{-1} as can be seen in Figure 5B. The isotope effect is difficult to discern in a difference spectrum because, for both DHP and HHMb, there is a large decrease in intensity associated with deuteration of the hydroxide adduct. Nonetheless, there are clearly two distinct bands that are evident in the DHP-OD and HHMb-OD spectra. The HRP-OH adduct has a ν_{Fe-OH} stretching mode at 503 cm^{-1} corresponding only to the LS species (*70*, *72*). The relative population of the high-spin and low-spin hydroxy species can also be estimated from resonance Raman spectra obtained in the high-frequency region as shown in Figure 6. Figure 6 shows that HHMb-OH is mainly HS, DHP-OH has significant contributions from both LS and HS, and HRP-OH is mostly LS. These observations are consistent with the above analysis of the Fe−OH stretching vibration.

The ν_4 band is also known as the electron density marker mode. It is sensitive to the oxidation state of the heme iron. It is noteworthy that in all of the adducts studied there is a trend for ν_4 to increase in frequency in the order ν_4(HRP) > ν_4(DHP) > ν_4(HHMb). This trend can be clearly seen in Figures 4, 5, and 7 for no axial ligand (or H_2O in the case of HHMb), F ligand, and OH ligand, respectively.

Density Functional Theory Calculations. Density function theory (DFT) calculations of a porphine model system shown in Figure 7 permit changes in spin state to be related to structural changes in core size. The model was geometry optimized in three spins, LS, IS, and HS, corresponding to $S = {}^1/_2$, $S = {}^3/_2$, and $S = {}^5/_2$, respectively. The core size can be defined in terms of the average Fe−Np distance and the Fe out-of-plane displacement. The Fe−Np bond distance was calculated to be 2.029, 2.036, and 2.080 Å, for LS, IS, and HS, respectively. The Fe out-of-plane displacement is 0.194, 0.206, and 0.302 Å, for LS, IS, and HS, respectively. The largest change occurs for the change from IS to HS. In the case of the 5-coordinate complex the highest energy d-orbital is the $d_{x^2-y^2}$, which is oriented toward the Fe−Np bonds. Only in the $S = {}^5/_2$, HS, state is there significant electron density in this orbital. This leads to the large repulsion between the iron and ring and the corresponding core size expansion. The effect of the spin state populations is manifested in differences in the Fe−N_ϵ bond length. Here the largest change occurs between the LS and IS spin states. The calculated Fe−N_ϵ bond lengths are 2.034, 2.199, and 2.187 Å, respectively, for the LS, IS, and HS states. The large increase in Fe−N_ϵ bond length occurs when the d_{z^2} orbital is occupied. It is clear from the DFT calculation that the d_{z^2} orbital lies below the $d_{x^2-y^2}$ in energy.

DISCUSSION

Raman scattering from the core size marker modes has been used as the basis for understanding the trends in spin states of ferric heme iron. The Soret band maxima show a less conclusive trend as indicated by comparison of the UV−vis absorption data in Table 1 with the Raman data in Tables 2−4. The resonance Raman data show that ligands of intermediate strength are bound to the heme iron. We hypothesize that the reason for the lack of a trend in the Soret band maxima is that the effect of axial ligation on the porphyrin π-system depends more strongly on the π-acid strength of the axial ligand than on the spin state. Ligands such as CN^- and N_3^- form LS adducts with Soret bands that are shifted to the range 421−423 nm (*6*, *7*). The OH^- and SCN^- and the halides have weaker ligation leading to varying amounts of HS and LS populations but also with distinctly less π-character. Their Soret band maxima fall in the range 412−414 nm. In the case of SCN^- the softer sulfur atom leads to poorer overlap. The hydroxide adduct likely depends on the hydrogen bonding. Compound II, which is a deprotonated hydroxy adduct, has a double bond and a Soret band at 419 nm in DHP (*5*). The halide adducts all have Soret bands around 406 nm in DHP and 407−409 nm in HHMb regardless of the spin state. Thus, the Soret band alone is not a good indicator of the spin state.

The correlation of the iron spin state and core size mode frequency is based on the coupling of the vibrational modes involving the heme periphery with strain located at the pyrrole nitrogens due to metal−porphyrin interactions. High-spin ($S = {}^5/_2$) iron has greater electron density in the $d_{x^2-y^2}$ orbital, which is directed toward the pyrrole nitrogens. This tends to force the iron further out of the heme plane. In addition, the Fe−N_p bond lengths increase as the core size expands. However, the high-spin heme iron can only partially relieve the strain of the expanded core size by an out-of-plane displacement. The expansion of the porphyrin ring leads to ring strain on the C_α−N_p bonds and on the C_α−C_m bonds. This strain lowers the frequencies of several key

vibrational modes, ν_2 (A_{1g}), ν_3 (A_{1g}), ν_{10} (B_{1g}), and ν_{11} (B_{1g}). There were early reports that ν_{19} (A_{2g}) was also affected (*50*, *51*). The vibronic modes (B_{1g} and A_{2g}) are easiest to observe using Q-band (α,β-band) excitation, while the A_{1g} modes are most prominent for Soret excitation. The origin of these different resonance Raman enhancements lies in the difference between a vibronic (Herzberg−Teller) mechanism for enhancement in the Q-bands and Frank−Condon enhancement in the Soret band. In spite of the fact that the Raman enhancement of the Soret band is dominated by totally symmetric modes that gain their Raman enhancement by origin displacements, there is a small degree of Herzberg−Teller enhancement in the Soret band. Weak bands such as the Q-band and charge-transfer bands gain in oscillator strength by vibronic coupling to the Soret band, and this in turn means that the Soret band takes on some of the character of the forbidden transitions (*73*−*75*).

We have used Soret band excitation to probe the change in spin state population for a series of heme iron ligands in the ferric form of DHP, HHMb, and HRP. Soret band excitation was first employed to determine the core size marker band frequencies by Callahan and Babcock (*50*, *51*), who showed that ν_3 was more readily distinguished than ν_2 or ν_{10} because it is in a less congested region of the Raman spectrum. Callahan and Babcock (*50*, *51*) did caution that use of ν_3 alone did not provide as good a correlation as what they called ν_{19} (but is now assigned as ν_2). However, Callahan and Babcock were measuring a number of different hemes with quite different peripheral substitution patterns (*50*, *51*). The present study focuses on the effects of protein structure and axial ligation on *b*-type hemes. There are differences in heme structure since heme doming (A_{2u}) tends to be the dominant distortion in globins, while heme saddling (B_{1u}) tends to be the dominant distortion in peroxidases (*52*). The ν_3 band is adequate for our comparisons and while comparisons based on ν_2 largely agree, there are complications because of the presence of modes ν_{11} and ν_{19} in this spectral region.

The halide series shows predictable progression from HS to LS for the DHP adducts. High-spin fluoride samples have 65%, 71%, and 92% of HS character as calculated from ν_3 for DHP, HHMb, and HRP, respectively. The chloride adducts DHP-Cl and HHMb-Cl have 36% and 70% HS character, respectively. Bromide adducts DHP-Br and HHMb-Br have 0% and 74% HS character, respectively, as calculated from ν_3. DHP is consistently lower spin throughout the halide series and for SCN adducts as shown in Tables 2 and 3.

The significance of the hydroxide adduct data is complicated. First, the deuterium isotope effect is unusual, consisting of a Raman band shift and a decrease in Raman band intensity. On the basis of the isotope shift there is one band peak at ~490 cm^{-1} that shows an isotope shift in both HHMb-OH and DHP-OH. Our data agree with other reports of a multicomponent band at 490 cm^{-1} (*54*, *69*). The temperature dependence of the Mb−OH band reveals a 560 cm^{-1} band that shows the isotope shift at 20 K and has been assigned as the LS component (*70*), which we have not verified in DHP. On the basis of these data the frequency of the Fe−OH stretch is slightly higher in DHP-OH than HHMb-OH, and the Fe−OH bond in DHP-OH is stronger than that in HHMb-OH in the HS form. As indicated in Scheme 1 there are two possible effects that can shift the Fe−OH frequency. For either an increase in hydrogen bond donation to the oxygen lone pair or a decrease in hydrogen bond acceptor strength with the O−H hydrogen, the interaction of OH^- with Fe(III) should weaken. In other words, the frequency of the Fe−OH stretch should increase as hydrogen bond donation weakens. Since the distal histidine of DHP is shifted approximately 1.5 Å farther from the heme than in myoglobin, the weaker hydrogen bonding in DHP-OH is expected to give rise to a stronger Fe−OH bond. The pK_a of 8.0 for formation of DHP-OH (*6*) is significantly lower than the pK_a for either HHMb-OH or HRP-OH. The pK_as of HHMb-OH and HRP-OH are 9.55 and 10.3, respectively (see also Supporting Information). Given that DHP and HHMb only have the distal histidine at high pH while HRP has both His42 and Arg38, it is somewhat surprising that formation of DHP-OH has such a low pK_a. It is reasonable to hypothesize that distal side hydrogen bond acceptor interactions are stronger in DHP than in HHMb, consistent with both the higher Fe−OH frequency and the lower pK_a for hydroxide adduct formation.

One of the most important states is the resting state of the enzyme (or globin). This is usually a 5-coordinate adduct. The frequencies of the 5-coordinate adducts of HRP and DHP are intermediate between the 6-coordinate HS and LS frequencies. This may arise from an intermediate-spin state as suggested elsewhere (*65*). According to DFT calculations there is a relatively small change in porphine ring structure for the LS → IS transition. There is a change in axial ligation due to electron repulsions with the electron d_{z^2}. As shown in Figure 7, the out-of-plane displacement of the iron and Fe−Np bond lengths increase mainly for the IS → HS transition. These factors suggest that a quantum mechanically mixed state proposed to explain the intermediate frequency of ν_3 in other peroxidases (*67*, *76*) may be a general feature of 5-coordinate ferric heme iron. Whether this is the explanation for DHP remains to be seen since there is conflicting evidence concerning the axial ligation in the ferric resting state. The X-ray structure indicates that the heme iron is 5-coordinate (*3*, *4*) while MCD (*31*), UV−vis titrations (*6*), and the resonance Raman data (this work) are consistent with a water molecule bound in the distal axial site.

CONCLUSION

The hypothesis that a protein can have the dual functions of a hemoglobin and a dehaloperoxidase presents a number of mechanistic challenges. The structure of DHP is consistent with the hemoglobin function, rather than a peroxidase function. DHP lacks the most important structural features found in all other heme peroxidases on both the proximal and distal side of the heme. The Asp-His-Fe charge relay is not present in DHP and is replaced by much weaker interactions on the proximal side. However, the proximal ligation in DHP is significantly stronger than in Mb based on the data obtained in this study, which show that the DHP spin state population is intermediate between HHMb and HRP. The measurement in this study relies on comparison of the ν_3 frequency for various ligand adducts. The combination of a distal His and Arg found in the distal pocket of peroxidases, such as HRP, is not observed in the DHP structure. The consequence of this difference can be seen in the similarity of the Fe−OH stretching mode in HHMb and

DHP. Both the distal and proximal structural features are thought to be essential for rapid activation of bound H_2O_2 to form compound I. In spite of these glaring differences, DHP has an enzymatic rate for oxidation of phenols that is at least an order of magnitude higher than any other known hemoglobin. These data are in agreement with DFT calculations (*63*), which indicate that a charge relay mechanism can function in DHP by means of a very strong hydrogen bond to a backbone carbonyl. These observations are consistent with a heme iron poised to act as both an oxygen-binding protein and an electron acceptor in the peroxidase reaction cycle. While there are many remaining questions regarding the nature of the DHP active site, a next step is to identify the factors that govern the switch of DHP function from an oxygen-binding protein to a peroxidase.

SUPPORTING INFORMATION AVAILABLE

Titration data for HHMb, DHP, and HRP acid−alkaline transitions and Raman spectra for DHP-Cl, DHP-Br, DHP-SCN, and DHP-N_3. This material is available free of charge via the Internet at http://pubs.acs.org.

REFERENCES

1. Chen, Y. P., Woodin, S. A., Lincoln, D. E., and Lovell, C. R. (1996) An unusual dehalogenating peroxidase from the marine terebellid polychaete *Amphitrite ornata*, *J. Biol. Chem. 271*.
2. Weber, R. E., Magnum, C. P., Steinman, H., Bonaventura, C., Sullivan, B., and Bonaventura, J. (1977) Hemoglobins of two terebellid polychaetes: *Enoplobranchus sanuigneus* and *Amphitrite ornata*, *Comp. Biochem. Physiol. 56A*, 179−187.
3. Lebioda, L., LaCount, M. W., Zhang, E., Chen, Y. P., Han, K., Whitton, M. M., Lincoln, D. E., and Woodin, S. A. (1999) An enzymatic globin from a marine worm, *Nature 401*, 445.
4. LaCount, M. W., Zhang, E. L., Chen, Y. P., Han, K. P., Whitton, M. M., Lincoln, D. E., Woodin, S. A., and Lebioda, L. (2000) The crystal structure and amino acid sequence of dehaloperoxidase from *Amphitrite ornata* indicate common ancestry with globins, *J. Biol. Chem. 275*, 18712−18716.
5. Belyea, J., Gilvey, L. B., Davis, M. F., Godek, M., Sit, T. L., Lommel, S. A., and Franzen, S. (2005) Enzyme function of the globin dehaloperoxidase from *Amphitrite ornata* is activated by substrate binding, *Biochemistry 44*, 15637−15644.
6. Nienhaus, K., Deng, P. C., Belyea, J., Franzen, S., and Nienhaus, G. U. (2006) Spectroscopic study of substrate binding to the carbonmonoxy form of dehaloperoxidase from *Amphitrite ornata*, *J. Phys. Chem. B 110*, 13264−13276.
7. Franzen, S., Jasaitis, A., Belyea, J., Brewer, S., Casey, R., MacFarlane, I. V., A. W., Stanley, R., Vos, M. H., and Martin, J.-L. (2006) NO-heme geminate recombination dynamics in dehaloperoxidase. *J. Phys. Chem. B 110*, 14483−14493.
8. Franzen, S., Dyer, R. B., Woodruff, W. H., Roach, M. R., Chen, Y. P., and Dawson, J. H. (1998) The unusual reactivities of *Amphitrite ornata* and *Notomastus lobatus* do not result from strong hydrogen bonding of their proximal histidine heme iron ligands, *J. Am. Chem. Soc. 120*, 4658−4661.
9. Royer, W. E., Jr., Pardanani, A., Gibson, Q. H., Peterson, E. S., and Friedman, J. M. (1996) Ordered water molecules as key allosteric mediators in a cooperative dimeric hemoglobin, *Proc. Natl. Acad. Sci. U.S.A. 93*, 14526−14531.
10. Ascenzi, P., Bocedi, A., de Sanctis, D., Pesce, A., Bolognesi, M., Marden, M. C., Dewilde, S., Moens, L., Hankeln, T., and Burmester, T. (2004) Neuroglobin and cytoglobin−Two new entries in the hemoglobin superfamily, *Biochem. Mol. Biol. Educ. 32*, 305−313.
11. Han, K. P., Woodin, S. A., Lincoln, D. E., Fielman, K. T., and Ely, B. (2001) *Amphitrite ornata*, a marine worm, contains two dehaloperoxidase genes, *Mar. Biotechnol. 3*, 287−292.
12. Suzuki, T., and Imai, K. (1998) Evolution of myoglobin, *Cell. Mol. Life Sci. 54*, 979−1004.
13. Matsui, T., Ozaki, S., Liong, E., Phillips, G. N., and Watanabe, Y. (1999) Effects of the location of distal histidine in the reaction of myoglobin with hydrogen peroxide, *J. Biol. Chem. 274*, 2838−2844.
14. Ozaki, S., Hara, I., Matsui, T., and Watanabe, Y. (2001) Molecular engineering of myoglobin: The improvement of oxidation activity by replacing Phe-43 with tryptophan, *Biochemistry 40*, 1044−1052.
15. Roach, M. P., Puspita, W. J., and Watanabe, Y. (2000) Proximal ligand control of heme iron coordination structure and reactivity with hydrogen peroxide: investigations of the myoglobin cavity mutant H93G with unnatural oxygen donor proximal ligands, *J. Inorg. Biochem. 81*, 173−182.
16. Egawa, T., Yoshioka, S., Takahashi, S., Hori, H., Nagano, S., Shimada, H., Ishimori, K., Morishima, I., Suematsu, M., and Ishimura, Y. (2003) Kinetic and spectroscopic characterization of a hydroperoxy compound in the reaction of native myoglobin with hydrogen peroxide, *J. Biol. Chem. 278*, 41597−41606.
17. Spiro, T. G., Smulevich, G., and Su, C. (1990) Probing protein structure and dynamics with resonance Raman spectroscopy: Cytochrome *c* peroxidase and hemoglobin. *Biochemistry 29*, 4497−4508.
18. Gajhede, M., Schuller, D. J., Henriksen, A., Smith, A. T., and Poulos, T. L. (1997) Crystal structure of horseradish peroxidase C at 2.15 angstrom resolution, *Nat. Struct. Biol. 4*, 1032−1038.
19. Tanaka, M., Ishimori, K., Mukai, M., Kitagawa, T., and Morishima, I. (1997) Catalytic activities and structural properties of horseradish peroxidase distal His42 → Glu or Gln mutant, *Biochemistry 36*, 9889−9898.
20. Poulos, T. L., and Kraut, J. (1980) The structure of cytochrome *c* peroxidase at 2.5 Å resolution, *J. Biol. Chem. 255*, 575−580.
21. Poulos, T. L., Edwards, S. L., Wariishi, H., and Gold, M. H. (1993) Crystallographic refinement of lignin peroxidase at 2 Å, *J. Biol. Chem. 268*, 4429−4440.
22. Schuller, D. J., Ban, N., van Huystee, R. B., McPherson, A., and Poulos, T. L. (1996) The crystal structure of peanut peroxidase, *Structure 4*, 311−321.
23. Mukai, M., Mills, C. E., Poole, R. K., and Yeh, S. R. (2001) Flavohemoglobin, a globin with a peroxidase-like catalytic site, *J. Biol. Chem. 276*, 7272−7277.
24. Goodin, D. B., and McRee, D. E. (1993) The Asp-His-Fe Triad of cytochrome *c* peroxidase controls the reduction potential, electronic structure, and coupling of the tryptophan free radical to the heme, *Biochemistry 32*, 3313−3324.
25. Vojtechovsky, J., Chu, K., Berendzen, J., Sweet, R. M., and Schlichting, I. (1999) Crystal structures of myoglobin-ligand complexes at near-atomic resolution, *Biophys. J. 77*, 2153−2174.
26. Parak, F., Hartmann, H., Aumann, K. D., Reuscher, H., Rennekamp, G., Bartunik, H., and Steigemann, W. (1987) Low-temperature X-ray investigation of structural distributions in myoglobin, *Eur. Biophys. J. Biophys. Lett. 15*, 237−249.
27. Shiro, Y., Iizuka, T., Marubayashi, K., Ogura, T., Kitagawa, T., Balasubramanian, S., and Boxer, S. G. (1994) Spectroscopic study of Ser92 mutants of human myoglobin−hydrogen bonding effect of Ser92 to proximal His93 on structure and property of myoglobin, *Biochemistry 33*, 14986−14992.
28. Lloyd, E., Burk, D. L., Ferrer, J. C., Maurus, R., Doran, J., Carey, P. R., Brayer, G. D., and Mauk, A. G. (1996) Electrostatic modification of the active site of myoglobin: characterization of the proximal Ser92Asp variant, *Biochemistry 35*, 11901−11912.
29. Svistunenko, D. A. (2005) Reaction of haem containing proteins and enzymes with hydroperoxides: the radical view, *Biochim. Biophys. Acta 1707*, 127−155.
30. Henricksen, A., Schuller, D. J., Meno, K., Welinder, K. G., Smith, A. T., and Gajhede, M. (1998) Structural interactions between horseradish peroxidase C and the substrate benzhydroxamic acid determined by X-ray crystallography, *Biochemistry 37*, 8054−8060.
31. Osborne, R. L., Sumithran, S., Coggins, M. K., Chen, Y. P., Lincoln, D. E., and Dawson, J. H. (2006) Spectroscopic characterization of the ferric states of *Amphitrite ornata* dehaloperoxidase and *Notomastus lobatus* chloroperoxidase: His-ligated peroxidases with globin-like proximal and distal properties, *J. Inorg. Biochem. 100*, 1100−1108.
32. Mukai, M., Nagano, S., Tanaka, M., Ishimori, K., Morishima, I., Ogura, T., Watanabe, Y., and Kitagawa, T. (1997) Effects of concerted hydrogen bonding of distal histidine on active site structures of horseradish peroxidase. Resonance Raman studies with Asn70 mutants, *J. Am. Chem. Soc. 119*, 1758−1766.

33. Smulevich, G., Mauro, J. M., Fishel, L. A., English, A. M., Kraut, J., and Spiro, T. G. (1988) Heme pocket interactions in cytochrome *c* peroxidase studied by site-directed mutagenesis and resonance Raman spectroscopy, *Biochemistry 27*, 5477−5485.
34. Newmyer, S. L., Sun, J., Loehr, T. M., and deMontellano, P. R. O. (1996) Rescue of the horseradish peroxidase His-170 → Ala mutant activity by imidazole: Importance of proximal ligand tethering, *Biochemistry 35*, 12788−12795.
35. Nissum, M., Neri, F., Mandelman, D., Poulos, T. L., and Smulevich, G. (1998) Spectroscopic characterization of recombinant pea cytosolic ascorbate peroxidase: Similarities and differences with cytochrome *c* peroxidase, *Biochemistry 37*, 8080−8087.
36. Poulos, T. L., and Kraut, J. (1980) The stereochemistry of peroxidase catalysis, *J. Biol. Chem. 255*, 8199−8205.
37. Hiner, A. N. P., Raven, E. L., Thorneley, R. N. F., Garcia-Canovas, F., and Rodriguez-Lopez, J. N. (2002) Mechanisms of compound I formation in heme peroxidases, *J. Inorg. Biochem. 91*, 27−34.
38. Dunford, H. B. (2001) How do enzymes work? Effect of electron circuits on transition state acid dissociation constants, *J. Biol. Inorg. Chem. 6*, 819−822.
39. Franzen, S. (2002) An electrostatic model for the frequency shifts in the carbonmonoxy stretching band of myoglobin: Correlation of hydrogen bonding and the Stark tuning rate, *J. Am. Chem. Soc. 124*, 13271−13281.
40. Yamaguchi, K., Watanabe, Y., and Morishima, I. (1992) Push effect on the heterolytic O−O bond cleaveage of peroxoiron(II) porphyrin adducts, *Inorg. Chem. 31*, 156−157.
41. Bizzarri, A. R., and Cannistraro, S. (1993) Solvent modulation of the structural heterogeneity in Fe(III) myoglobin samples—a low-temperature EPR investigation, *Eur. Biophys. J. Biophys. Lett. 22*, 259−267.
42. Kitagawa, T., Nagai, K., and Tsubaki, M. (1979) Assignment of the Fe−Nϵ (His F8) stretching band in the resonance Raman spectra of deoxy myoglobin, *FEBS Lett. 104*, 376−378.
43. Bonagura, C. A., Bhaskar, B., Shimizu, H., Li, H. Y., Sundaramoorthy, M., McRee, D. E., Goodin, D. B., and Poulos, T. L. (2003) High-resolution crystal structures and spectroscopy of native and compound I cytochrome *c* peroxidase, *Biochemistry 42*, 5600−5608.
44. Nienhaus, K., Olson, J. S., Franzen, S., and Nienhaus, G. U. (2005) The origin of stark splitting in the initial photoproduct state of MbCO, *J. Am. Chem. Soc. 127*, 40−41.
45. Phillips, G. N., Jr., Teodoro, M. L., Li, T., Smith, B., and Olson, J. S. (1999) Bound CO is a molecular probe of the electrostatic potential in the distal pocket of myoglobin, *J. Phys. Chem. B 103*, 8817−8829.
46. Morikis, D., Champion, P. M., Springer, B. A., and Sligar, S. G. (1989) Resonance Raman investigations of site-directed mutants of myoglobin—Effect of distal histidine replacement, *Biochemistry 28*, 4791−4800.
47. Yang, F., and Phillips, G. N., Jr. (1996) Crystal structures of CO-, deoxy- and met-myoglobins at various pH values, *J. Mol. Biol. 256*, 762−774.
48. Franzen, S., Belyea, J. L., Gilvey, L. B. G., Davis, M. F., Chaudhary, C., Sit, T. L., and Lommel, S. A. (2006) Proximal cavity, distal histidine and substrate hydrogen-bonding mutations modulate the activity of *Amphitrite ornata* dehaloperoxidase, *Biochemistry 45*, 9085−9094.
49. Neri, F., Kok, D., Miller, M. A., and Smulevich, G. (1997) Fluoride binding in hemoproteins: The importance of the distal cavity structure, *Biochemistry 36*, 8947−8953.
50. Callahan, P. M., and Babcock, G. T. (1981) Insights into heme structure from Soret excitation Raman spectroscopy, *Biochemistry 20*, 952−958.
51. Morikis, D., Champion, P. M., Springer, B. A., Egeberg, K. D., and Sligar, S. G. (1990) Resonance Raman studies of iron spin and axial coordination in distal pocket mutants of ferric myoglobin, *J. Biol. Chem. 265*, 12143−12145.
52. Choi, S., Spiro, T. G., Langry, K. C., Smith, K. M., Budd, L. D., and LaMar, G. N. (1982) Structural correlations and vinyl influences in resonance Raman spectra of protoheme complexes and proteins, *J. Am. Chem. Soc. 104*, 4345−4351.
53. Jentzen, W., and Shelnutt, J. A. (1997) The conformation of the heme is conserved in proteins of the same functional class, *Biophys. J. 72*.
54. Desbois, A., Lutz, M., and Banerjee, R. (1979) Low-frequency vibrations in resonance Raman spectra of horse heart myoglobin. Iron-ligand and iron-nitrogen vibrational modes, *Biochemistry 18*, 1510−1518.
55. Spiro, T. G., Stong, J. D., and Stein, P. (1979) Porphyrin core expansion and doming in heme proteins. New evidence from resonance Raman spectra of six-coordinate high-spin iron(III) hemes, *J. Am. Chem. Soc. 101*, 2648−2655.
56. Franzen, S., Lambry, J. C., Bohn, B., Poyart, C., and Martin, J. L. (1994) Direct evidence for the role of heme doming as the primary event in the cooperative transition of hemoglobin, *Nat. Struct. Biol. 1*, 230−233.
57. Perdew, J. P., Chevary, J. A., Vosko, S. H., Jackson, K. A., Pederson, M. R., Singh, D. J., and Fiolhais, C. (1992) Atoms, molecules, solids and surfaces—Applications of the generalized gradient approximation for exchange and correlation, *Phys. Rev. B 46*, 6671−6687.
58. Delley, B. (1990) *J. Chem. Phys. 92*, 508−517.
59. Delley, B. (2000) From molecules to solids with the DMol(3) approach, *J. Chem. Phys. 113*, 7756−7764.
60. Mermin, D. (1965) *Phys. Rev. A 137*, 1441−1443.
61. Franzen, S., Fritsch, K., and Brewer, S. H. (2002) Experimental observation of anharmonic coupling of the heme-doming and iron-ligand out-of-plane vibrational modes confirmed by density functional theory, *J. Phys. Chem. B 106*, 11641−11646.
62. Franzen, S. (2002) Spin-dependent mechanism for diatomic ligand binding to heme, *Proc. Natl. Acad. Sci. U.S.A. 99*, 16754−16759.
63. Franzen, S. (2001) Effect of a charge relay on the vibrational frequencies of carbonmonoxy iron porphine adducts: The coupling of changes in axial ligand bond strength and porphine core size, *J. Am. Chem. Soc. 123*, 12578−12589.
64. Neri, F., Indiani, C., Baldi, B., Vind, J., Welinder, K. G., and Smulevich, G. (1999) Role of the distal phenylalanine 54 on the structure, stability, and ligand binding of *Coprinus cinereus* peroxidase, *Biochemistry 38*, 7819−7827.
65. Wang, M.-Y., and Hoffman, B. M. (1994) Systematic trends in metalloporphyrin optical spectra, *J. Am. Chem. Soc. 106*, 4235−4240.
66. Zerner, M., Gouterman, M., and Kobayashi, H. (1966) Porphyrins VIII. Extended Huckel calculations on iron complexes. *Theor. Chim. Acta 6*, 363−400.
67. Howes, B. D., Schiodt, C. B., Welinder, K. G., Marzocchi, M. P., Ma, J. G., Zhang, J., Shelnutt, J. A., and Smulevich, G. (1999) The quantum mixed-spin heme state of barley peroxidase: A paradigm for class III peroxidases, *Biophys. J. 77*, 478−492.
68. Hoard, J. L. (1975) *Porphyrins and Metalloporphyrins* (Smith, K. M., Ed.) Elsevier, Amsterdam.
69. Asher, S. A., and Schuster, T. M. (1979) Resonance Raman Examination of axial ligand bonding and spin-state equilibria in metmyoglobin hydroxide and other heme derivatives, *Biochemistry 18*, 5377−5387.
70. Feis, A., Marzocchi, M. P., Paoli, M., and Smulveich, G. (1994) Spin state and axial ligand bonding in the hydroxide complexes of metmyoglobin, methemoglobin, and horseradish peroxidase at room and low temperatures, *Biochemistry 33*, 4577−4583.
71. Shelnutt, J. A., Alden, R. G., and Ondrias, M. R. (1986) Heme-linked ionization in horseradish peroxidase detected by Raman difference spectroscopy, *J. Biol. Chem. 261*, 1720−1723.
72. Sitter, A. J., Shifflett, J. R., and Terner, J. (1988) Resonance Raman spectroscopic evidence for heme iron-hydroxide ligation in peroxidase alkaline forms, *J. Biol. Chem. 263*, 13032−13038.
73. Franzen, S., Morre, L. J., Woodruff, W. H., and Boxer, S. G. (1999) Stark effect spectroscopy of the heme charge transfer bands of deoxymyoglobin, *J. Am. Chem. Soc. 121*, 3070−3072.
74. Franzen, S., Wallace-Williams, S. E., Shreve, A. P., and Dyer, R. B. (2002) Heme charge-transfer band III is vibronically coupled to the soret band, *J. Am. Chem. Soc. 124*, 7146−7155.
75. Franzen, S. (2002) Perimeter model for the magnetic circular dichroism spectrum of deoxy ferrous heme in myoglobin, *J. Phys. Chem. B 106*, 10482−10491.
76. Indiani, C., Feis, A., Howes, B. D., Marzocchi, M. P., and Smulevich, G. (2000) Effect of low temperature on soybean peroxidase: spectroscopic characterization of the quantum-mechanically admixed spin state, *J. Inorg. Biochem. 79*, 269−274.

BI0609218